2023 IEEE/ASME International Conference on Advanced Intelligent Mechatronics (AIM)
June 28-30, 2023. Seattle, Washington, USA

Aerial Deployment of Novel Gravity-Assisted Ground Penetrating Sensors using Nature-Inspired Platform

Shane Kyi Hla Win, Kristabel Lim, Brian Leonard Suhadi, Danial Sufiyan and Shaohui Foong

***Abstract*— This paper explores an aerial deployment of sensors which are intended to penetrate into the ground upon impact, enabling data collection of ground properties such as soil moisture, temperature and salinity. This is made possible by the use of diving Samara Autorotating Wing (dSAW), explored in our previous work, which uses a single actuator to perform both a guided autorotation and diving towards the ground at terminal velocity. The versatile maneuvers of dSAW allows a special deployment method whereby the platform can navigate and glide towards intended location and perform a ground insertion of a sensor using its dive. In this work, the feasibility of such deployment is tested using an indoor test rig which accelerates sensors towards a test soil. The prototypes carrying sensors are dropped at a maximum of 15ms^{-1} into three different soil types and different levels of moisture and its moment of impact is captured by a high-speed camera at 5,000fps. The sensor selected is shown to survive all drop scenarios, hence demonstrating the feasibility of aerially deployed ground penetrating sensors.**

I. Introduction

A large scale of sensor networks distributed over an expansive remote area may form the basis for systems such as environmental monitoring [1], population surveillance and climate detection [2] [3] in the near future. Manually installing such sensor networks could be an expensive and labor intensive process that does not scale well for a large distribution of sensors especially in remote or dangerous locations.

Aerial distribution methods could be a viable solution to deploy large scale sensor networks [4]–[11]. Small sensors can be packaged, carried by aircraft and airdropped over regions of interest. Unmanned Aerial Vehicles (UAV) can be used for airdropping sensors as well, which can automate the entire deployment process. As for the sensor's journey towards the ground upon being airdropped, some research have looked at nature for inspiration, making sensors float slowly towards the ground similar to dandelions [10] [11], or autorotate similar to maple seeds [5] [6] [9]. Other works have focused on achieving controlled flight trajectories so as to precisely place sensors in intended locations [5] [6] [8].

In our recent works [4]–[6], we have introduced a samara-inspired aerial sensor deployment method, called the Samara Autorotating Wing (SAW), shown in Fig. 1(B). It is a simple mono-wing which borrows from the shape of maple seeds. It is equipped with a micro-controller, a battery, a magnetometer, a GPS, an actuator and potentially a small sensor payload. Its trajectory control is achieved by actuating a flap cyclically as it autorotates towards the ground. In [6], a new flight method, the 'dive', was introduced in order to descend quickly through high winds or simply to reach the ground faster. The proposed prototype could switch between autorotation and dive within a short period of time and also without needing an additional actuator, as shown in Fig. 1.

In this paper, we propose a method to deploy sensors that penetrate or are inserted into the ground. This method takes advantage of the diving mode of dSAW, whereby it accelerates towards the ground using only gravity similar to a free-falling arrow. Based on our previous tests, its dive can reach up to 25 ms^{-1}. By attaching a ruggedized sensor which can withstand the impact of landing at high speed, we can potentially deploy sensors that needs to be underneath the surface of soil. As dSAW has guided trajectory, it can steer itself towards an intended location and enter a dive for its final maneuver.

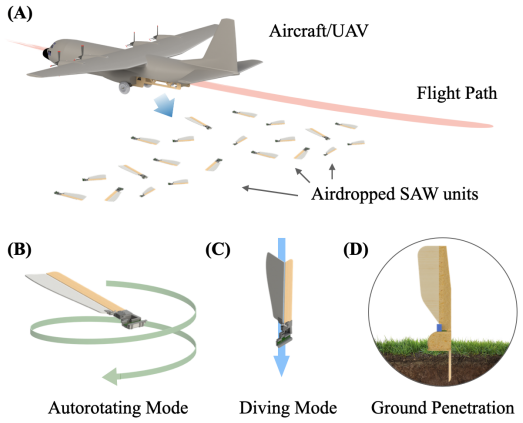

Fig. 1. (A) An aircraft or UAV deploying several dSAW units at once; (B) dSAW unit in autorotating mode whereby it has a gentle descent and controlled glide direction; (C) dSAW unit in diving mode whereby it can descend about 18 times faster than its descent speed in autorotating mode; (D) A proposed ground-penetrating sensor deployment method.

The contributions of this work are as follows -

- We propose a method to aerially deploy guided sensors which penetrate into the ground.
- An indoor test setup to repeatedly launch sensors into a controlled soil is proposed, and the design process of the test setup is outlined. This setup uses simple aluminum extrusion frames and utilizes stored elastic energy from exercise rubber bands to launch the sensor into the soil at high speed.
- An experiment is carried out to test the durability of a selected soil moisture sensor by launching it high speed

The authors are with Engineering Product Development Pillar, Singapore University of Technology & Design (SUTD), 8 Somapah Road, Singapore 487372. (Corresponding e-mail: foongshaohui@sutd.edu.sg)

into three different types of soil at various moisture levels. Its descent is tracked using motion-tracking system to calculate its impact velocity and the impact moment is recorded with a high speed camera at 5,000fps for visual observation.

II. Design Concept

Samara Autorotating Wing (SAW) platform has proved to be a versatile and low-cost aerial deployment platform for lightweight sensors in our previous works [5] [6]. Regardless of its initial condition, it is able to enter a passively stable autorotation similar to the dynamical properties of its natural cousin, the maple seed. This means that it can be deployed by any aerial platform, regardless of fixed-wing or rotary-wing type, and it can begin autorotating as soon as it is released without the need for complex sensors or control algorithms for stabilization. As it requires only one actuator, a magnetometer and a GPS for its autonomous navigation, its cost is reasonably low, opening up the possibility of mass manufacturing and single-use scenarios. The single actuator on-board controls the angle of attack of the flap γ following the square cyclic control law denoted by -

$$\gamma = \begin{cases} \gamma_o + \gamma_{amp}, & \text{if } \sin(\theta_z + \lambda_c) > \epsilon \\ \gamma_o - \gamma_{amp}, & \text{if } \sin(\theta_z + \lambda_c) < -\epsilon \\ \gamma_o, & \text{otherwise} \end{cases} \quad (1)$$

where γ_o is the offset or neutral point, γ_{amp} is the amplitude, θ_z is the current azimuth angle, λ_c is the direction control input from human controller, and ϵ is the threshold that controls the duty cycle [6]. A 58g prototype using this control law is controllable in omni-direction achieving glide angle of 28.9° (measured from horizontal) while it is also capable of vertical descent at either 1.43 ms^{-1} or a free-falling 25 ms^{-1}, enabled when $\gamma = \pm 90°$. In the former speed, it can deploy sensors with a soft landing where the sensor may be sensitive to shock or when landing on soft structures such as vegetation. In the latter speed, it is ideal for deployment of sensors which needs to penetrate the ground. It is this mode of deployment that is explored further in this work.

By diving into the ground, the platform uses all its accumulated kinetic energy to push into the soil. Furthermore, it is oriented in a vertical manner which can be convenient for other purposes as shown in Fig. 2. Its wing can house solar cells which can harvest energy during daytime for extended operations which can span over months or even years. The vertical orientation of its wing also is ideal for integration of antenna for wireless communication, such as transferring data to other units, forming a swarm network in a remote deployment scenario. Its ground-penetrating component can be ruggedized to house a sensor or it can simply use a ruggedized sensor which can withstand the impact of ground collision. As the platform is only partially submerged in ground, its above-ground portion may still house a sensor for other purposes.

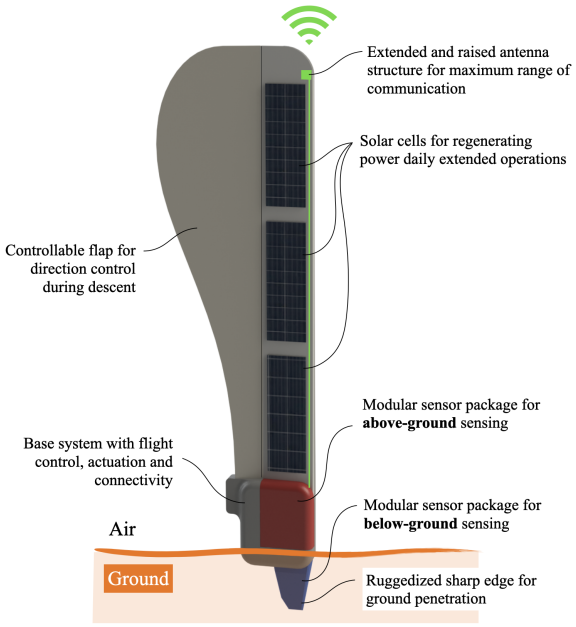

Fig. 2. Conceptual ground-penetrating sensor deployment using Samara Autorotating Wing concept.

III. Indoor Test Setup

It is difficult to perform a repeated test of airdropping a dSAW prototype, steering it towards an intended test site with sufficient height and making it dive into a controlled selection of soil monitored by our motion tracking cameras and visual cameras. Thus, an indoor test setup is favorable, which allows it to be placed within a motion-tracking setup and the impact can be recorded by a high speed camera in close proximity. The indoor test setup also facilitates similar conditions for repeated tests, while changing only the controlled parameters such as the soil type and moisture.

An indoor test setup requires acceleration of a test prototype (with sensor) to free-fall speeds of dSAW within an allowable space. In order to have a realistic penetration into soil, the test prototype must be accelerated vertically and dropped. As the indoor ceiling height is about 2.3m, the test rig must fit within a usable space of about 2m of height.

Figure 3(A) shows the indoor test setup created for this purpose. It is built from a simple arrangement of 30x30 aluminium extrusions. The structure is 2m tall, and occupies 0.5m x 0.5m of footprint, with laterally elongated legs for improved stability. Within the frame, a carriage is designed to push the prototype to its intended velocity. Two sets of elastic bands (exercise resistance bands) are attached to the carriage for the purpose of accelerating and decelerating it. The downward-pulling bands provide the necessary force for acceleration while the upward-pulling bands help slow down the carriage before it slams into a stopper. A plastic box filled with controlled soil sample is placed within the target area below the carriage. In this figure, the carriage is resting at its equilibrium, a short distance above its lower travel limit, receiving equal forces from both the downward-pulling band

and upward-pulling band.

Figure 3(B) shows the side view of the test setup. In a test operation, the carriage is pushed up to its loaded position and locked in place. At this point, the upward-pulling bands are completely relaxed while the downward-pulling bands are stretched at maximum. Upon release, the carriage accelerates towards the floor. After accelerating for about 0.87m, the upward-pulling bands begin to have tension and start providing decelerating force. The carriage decelerates for about 0.18m before hitting its end stop. At this point, the test prototype begins its separation from the carriage and free falls towards the soil below.

Figure 4 shows a close-up side view of the carriage. The carriage consists of a 3D-printed structure (Onyx material, Markforged Mark Two printer) which hugs around a linear bearing (Part number LKBM16UUOP, Misumi) and a vertical aluminium extrusion. This bearing moves smoothly along a 16mm steel shaft. On the carriage's rear, a locking pin is inserted to lock the carriage at its desired position using holes drilled onto the extrusion. This pin is pulled out manually to release the carriage. Carabiners are used to attach the elastic bands to the carriage, allowing easy change and replacement of bands if different strength of bands is desired. The attachment location is also strategically designed such that it is coincident to the steel shaft, hence no twisting torque would be applied to the carriage during its vertical travel. A set of shock absorbing bumpers (Part number GELP30, Misumi) is attached to both the end stop and the carriage, intended to absorb some of the residual impact as the carriage collides with the end stop after decelerating.

The test prototype consists of a 3D-printed structure, a soil moisture sensor at the bottom, steel weights attached near its base and a guiding tail. The purpose of the prototype is to provide a simple test platform to investigate the durability of the sensor while providing similar mechanical characteristics as the dSAW unit, thus weighing similarly to a single unit of dSAW (about 60g). The prototype is attached to the carriage by means of a small amount of friction. Two small steel rods extend vertically from the carriage which slots into the 3D-printed structure of the prototype, with a smooth tolerance fit. The guiding tail ensures proper alignment and orientation of the test prototype as it departs from the carriage. The arrangement of the two parallel steel rods and guiding tail are designed to ensure the orientation of the sensor is similar to that in actual practice.

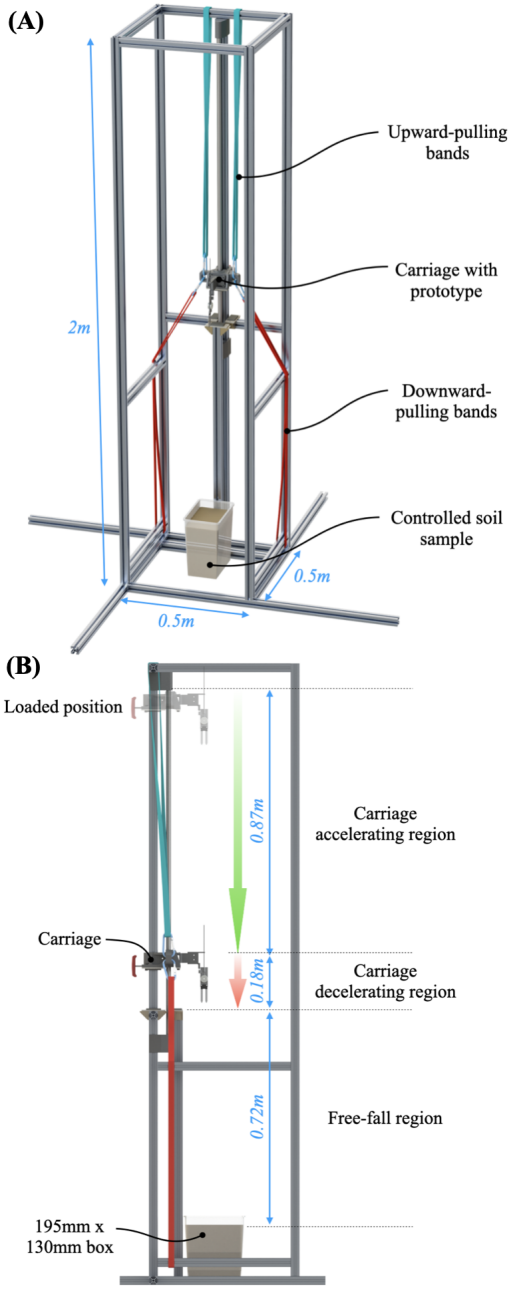

Fig. 3. (A) An isometric view of the indoor test setup, clearly showing arrangement of all major components; (B) A side view of the indoor test setup, depicting the carriage accelerating and decelerating regions, and the prototype free-fall region.

A. Elastic Band Selection

Elastic bands are used to provide the necessary force to launch the test prototype at required speeds. As the carriage is mounted on a linear bearing moving along a single steel shaft, two elastic bands are used for each direction of pull in order to ensure no twisting of the carriage is resulted from the elastic forces.

Five levels of strength of elastic bands are selected for possible use in this order - green, yellow, orange and red which are rated for 15kg, 25kg, 35kg and 45kg of resistance respectively. The elastic bands are characterized by stretching to the extension achieved by moving the carriage to loaded position, which is about 0.7m of extension. The resulting elastic constant k, shown in Table I and measured in Fig. 5, is computed using Hooke's Law given by -

$$F = kx \tag{2}$$

where F is the elastic force, k is the elastic constant and x is the extended distance. Next, potential energy E stored in the elastic band can be computed using the following equation -

$$E = \frac{1}{2}kx^2. \tag{3}$$

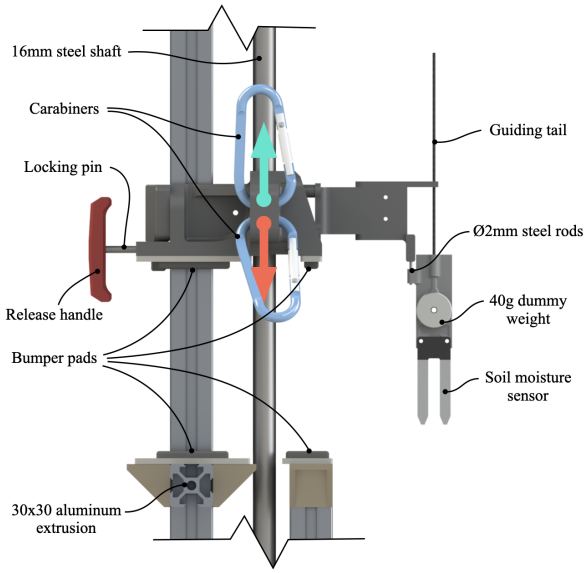

Fig. 4. A close-up side view of the carriage.

TABLE I
TABLE OF COMPARISON FOR ELASTIC BANDS

Band Color	Rated Strength	Measured k (N/m)	E (J)
Green	15 kg	117	28.7
Yellow	25 kg	206	50.5
Orange	35 kg	236	57.8
Red	45 kg	322	78.9

It can be assumed that the energy stored in the two accelerating elastic bands would be converted to the kinetic energy of the carriage assembly with some losses to heat and sound energies caused by friction. The efficiency of this energy conversion will be investigated in Section IV.

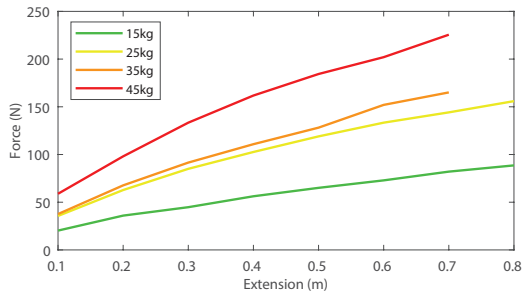

Fig. 5. Measured force versus extension plot for elastic bands of different strengths

B. Soil Types

Three different types of soil are prepared for testing. They are garden soil, sand and burnt soil as shown in Fig. 6.

Garden soil is a type of topsoil that has extra organic matter, such as compost, peat, bark shredding or fertilizer. It is relatively easy to obtain from gardening shops, and among the three types, it is the softest and easiest to penetrate into.

Sand is a naturally occurring granular material composed of finely divided rock and mineral particles. It is defined by size, being finer than gravel and coarser than silt. The most common component of sand is silicon dioxide in the form of quartz. Among the three types, it is tougher than garden soil to penetrate through.

Burnt soil is heavy and sticky clay that has been heat-treated to change its structural properties. The essential qualities of burnt soil are that it will absorb water without becoming sticky and that the lumps do not readily break down when the soil is watered. Normally, it contains large pieces of rock but for the experiment purpose, most of the rock is filtered out and only a fine powder is left.

Fig. 6. (A) Garden soil, (B) Sand and (C) Burnt Soil

C. Sensor Selection

There are several types of sensors that are used for measurements below-ground and most are related to measuring the various properties of soil. They are soil moisture sensor which measures the water content in soil, soil temperature sensor for measuring temperature of soil at various depths, soil conductivity sensor to measure the electrical conductivity of soil which can provide information on soil salinity and fertility, soil respiration sensor which measures the exchange of carbon dioxide between soil and the atmosphere to indicate soil health and rate of organic matter decomposition, soil gas sensor to measure gases such as carbon dioxide and methane in soil to understand microbial activity and soil compaction sensor to measure soil density and hardness. There are also sensors to measure soil pH, soil nutrient levels, soil erosion and earth movement.

Among all the sensors, we decided to use soil moisture sensors for this work as they are simple, robust and require the least modification. Soil moisture sensors work by measuring electrical resistance of soil to determine its water content. The sensor consists of two electrodes which are placed in the soil and connected to an electrical circuit. A small voltage is applied across the electrodes measuring the electrical resistance of the soil, which is then converted into a moisture content reading. The structure of the sensor is very simple with two electrodes formed by a single circuit board. As the sensor is low cost, it is easily replaced if broken during the experiments.

IV. Experimental Investigation

The experimental investigations is composed of two subsections - elastic band testing and drop tests. A high speed camera (Photron FASTCAM Mini UX100) is used to capture

the moment of impact at 5,000 fps. A motion tracking camera system (OptiTrack) is also used to capture the drop at 180 fps.

A. Elastic Band Testing

The carriage assembly with the prototype weighs a total of 650g. If the strongest (Red) elastic band is used, total energy stored in the pair of bands is 157.8J. Assuming all elastic energy is converted to kinetic energy ($E = \frac{1}{2}mv^2$) and also assuming assistance from gravity is negligible due to the very brief moment of acceleration, the carriage assembly would reach a velocity of 22 ms^{-1}. In reality, the maximum speed reached was approximately 15 ms^{-1}, hence about 53.6% of the stored elastic energy is lost to friction in the form of heat and sound. In the subsequent experiments, the red elastic band was used for downward-pulling and the the green band was used for upward-pulling.

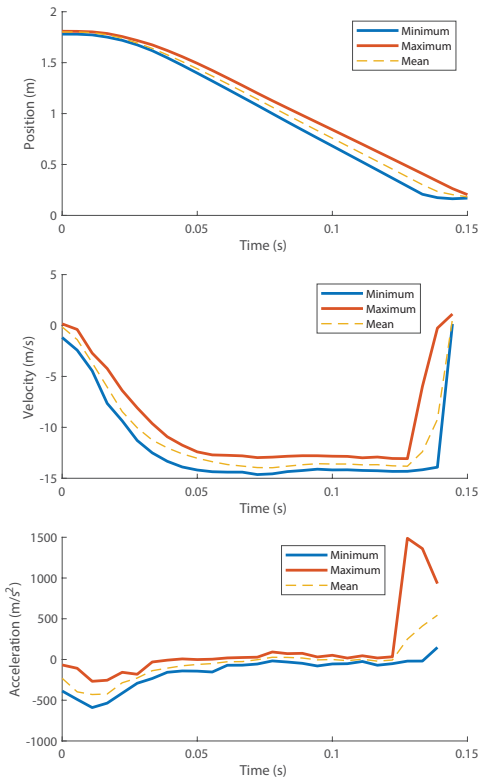

Fig. 7. Height, velocity and acceleration plots as measured by motion-tracking system for 15 drop tests.

B. Drop Tests

Drop tests were carried out on the three different soil samples on two scenarios - one on default soil moisture and one with moisture increased till the sensor reading is saturated. Water is added manually into the soil and the soil is mixed thoroughly to ensure even moisture content within the entire volume of the soil.

An infra-red reflective marker is placed on the prototype for motion-tracking. Figure 7 shows the position, velocity and acceleration of the prototype extracted from motion-captured data. Each drop had a duration of roughly 1.3s where the prototype is accelerated from rest, free falls at its peak velocity and impacts the soil. The peak velocity achieved during drops was 14.6 ms^{-1}. For most drops, the IR marker gets covered beneath the soil and the system loses its tracking on the prototype. On the drops where the IR marker does not get covered, a peak deceleration value can be measured and it is about 1487 ms^{-2}. It means that the sensor has to survive an impact of 151 Gs.

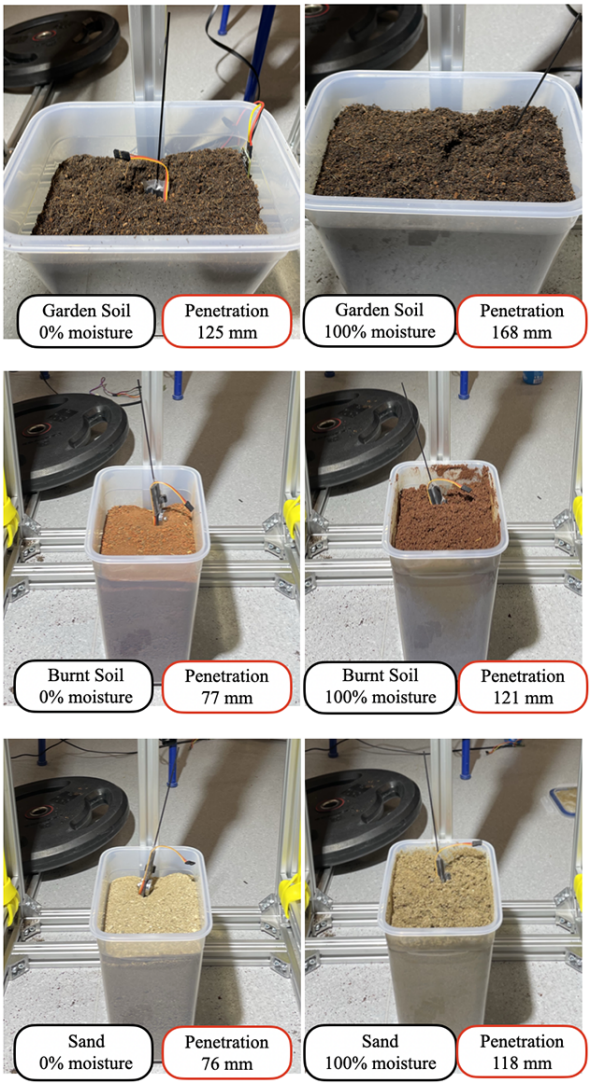

Fig. 8. Final resting position of the prototype in each of the three soils in different moisture conditions.

Figure 8 shows the final resting position of the prototype within different soil types, one with no added moisture and one with full moisture. In all cases, the prototype is able to penetrate through the soil without breaking. When the soil is at full moisture, it is easier for the prototype to penetrate through and submerges deeper. In all tests, the sensor is fully submerged at final resting position. The garden soil was easiest to penetrate through while the burnt soil and sand are about similarly harder for the sensor to penetrate.

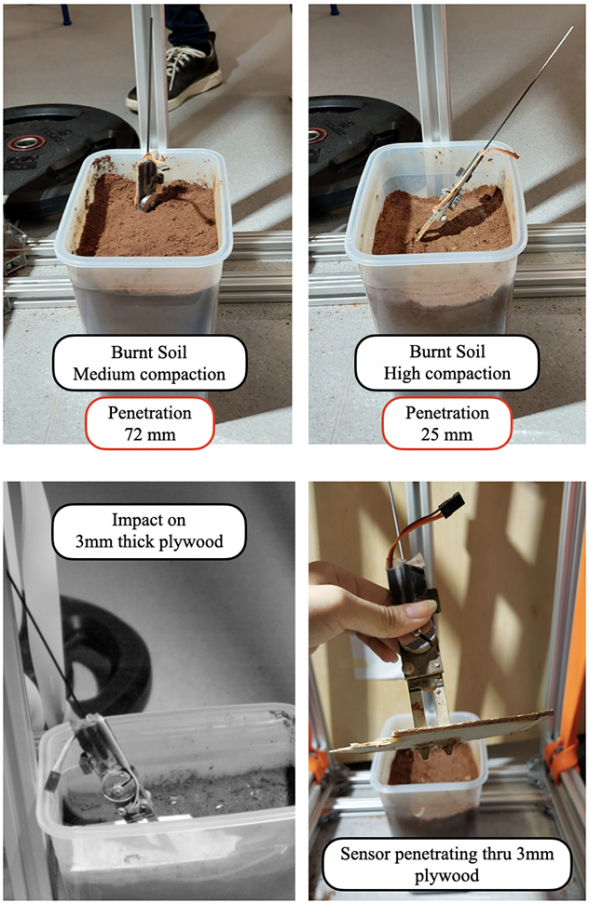

Fig. 9. Top: Test drops into burnt soil with increased compaction. Medium and high compaction are 6.2% and 20.5% increase in density respectively from original. Bottom: Test drop onto a small piece of 3mm thick plywood.

As the sensor was able to survive through all the drops, next was to test with increased compaction of the soil. The burnt soil was chosen to be compacted, to medium and high level of compaction achievable by manual compaction. The drop test was repeated on the two levels of compaction (Fig. 9). At high compaction, only about 25mm of the sensor (50% of its leg) penetrates the soil. As the sensor survived the compaction test, a small piece of 3mm thick plywood is placed on top of the soil to see if the sensor breaks if landed upon harder materials. As Fig. 9 shows, it is also able to survive this landing by penetrating into the plywood.

The videos captured by our high speed camera is presented in the supplementary materials. Figure 10 shows a sequence of images extracted from the video of one of the drop tests.

Fig. 10. Sequence of images extract from high speed video during the moment of impact of sensor and soil.

Although our experiment results are highly repeatable, there are some limitations to this approach. For instance, the test rig allows for reaching maximum drop velocity of about 15 ms^{-1} whereas in practice, dSAW may dive up to 25 ms^{-1}. It is likely that the sensor will survive the impact at latter speed, as it survived drop onto hard surfaces such as ply wood. Further tests in real-world conditions are necessary to verify its robustness.

V. Conclusions

In this paper, we have introduced a novel method to deploy ground-penetrating sensors using an aerial guided Samara Autorotating Wing platform. In order to test the feasibility of this method, we selected soil moisture sensor as a test sensor to penetrate the ground at high speeds. A special indoor test rig is built to demonstrate the high speed deployment scenario and the sensor mounted on a test prototype is launched at an average of 14.0 ms^{-1} into three different types of soil at different moisture levels, and the impact moment is captured using a high speed camera and a motion tracking system. The results show that deployment of ground-penetrating sensor is feasible using proposed method.

Acknowledgment

The authors would like to thank Mr. Sunny Deshpande Nitin, Mr. Joshua Tan Hiang Khai and Mr. Soon Yee Ho for their assistance in setting up the test rig.

References

[1] J. Jin, Y. Wang, H. Jiang, X. Chen, "Evaluation of microclimatic detection by a wireless sensor network in forest ecosystems," *Scientific Reports*, vol. 8, no. 1, pp. 1-9, 2018.

[2] J. Toledo-Castro, P. Caballero-Gil, I. Santos-Gonzalez, C. Hernandez-Goya, and R. Aguasca-Colomo, "Forest fire prevention, detection, and fighting based on fuzzy logic and wireless sensor networks," *Complexity*, vol. 12, pp. 1-17, 2018.

[3] G. Werner-Allen, J. Johnson, M. Ruiz, J. Lees, and M. Welsh, "Monitoring volcanic eruptions with a wireless sensor network," in *The Second European Workshop on Wireless Snesor Networks*, pp. 108-120, 2005.

[4] S.K.H. Win, T.H. Goh, J.E. Low, D.S.B. Shaiful, L.T.S. Win, G.S. Soh, S. Foong, "Direction controlled descent of Samara Autorotating Wings (SAW) with N-Wings," in Proceedings of IEEE International Conference on Robotics and Automation, 2018, pp. 6553-6559.

[5] S.K.H. Win, L.S.T. Win, D. Sufiyan, G. S. Soh, and S. Foong, "Dynamics and control of a collaborative and separating descent of samara autorotating wings," *IEEE Robotics and Automation Letters*, vol. 4, no. 3, pp. 3067-3074, 2019.

[6] S.K.H. Win, L.S.T. Win, D. Sufiyan, G.S. Soh and S. Foong, "An agile samara-inspired single-actuator rotary wing micro aerial vehicle," in *IEEE Transactions on Robotics*, Vol 38(2), pp. 1033-1046, 2021.

[7] V. Iyer, M. Kim, S. Xue, A. Wang, S. Gollakota, "Airdropping sensor networks from drones and insects," *MobiCom '20: Proc. 26th Annu. Intl Conf. Mobile Computing and Networking*, 61, pp. 1-14, 2020.

[8] D.J. Edwards, A.D. Kahn, S.B. Heinzen, T.Z. Young, N.J. Arnold, D. Newton, B. Eber and S.V. Carter, "CICADA flying circuit board unmanned aerial vehicle," *2018 AIAA Aerospace Sciences Meeting 1008*, 2018.

[9] P. Pounds, S. Singh, "Samara: biologically inspired self-deploying sensor networks," *IEEE Potentials*, Vol 34(2), pp. 10-14, 2015.

[10] V. Iyer, H. Gaensbauer, T.L. Daniel, S. Gollakota, "Wind dispersal of battery-free wireless devices," *Nature*, Vol 603, pp. 427-433, 2022.

[11] B.H. Kim et. al., "Three-dimensional electronic microfliers inspired by wind-dispersed seeds," *Nature*, Vol 597, pp. 503-510, 2021.